AFRL-VA-WP-TP-2006-322

BEAMFORMING OF LAMB WAVES FOR STRUCTURAL HEALTH MONITORING (PREPRINT)

Steven E. Olson, Martin P. DeSimio, and Mark M. Derriso

APRIL 2006

Approved for public release; distribution is unlimited.

STINFO COPY

AIR VEHICLES DIRECTORATE
AIR FORCE MATERIEL COMMAND
AIR FORCE RESEARCH LABORATORY
WRIGHT-PATTERSON AIR FORCE BASE, OH 45433-7542

REPORT DOCUMENTATION PAGE

Form Approved
OMB No. 0704-0188

1. REPORT DATE *(DD-MM-YY)*	2. REPORT TYPE	3. DATES COVERED *(From - To)*
April 2006	Journal Article Preprint	04/15/2005– 04/15/2006

4. TITLE AND SUBTITLE

BEAMFORMING OF LAMB WAVES FOR STRUCTURAL HEALTH MONITORING (PREPRINT)

5a. CONTRACT NUMBER
In-house

5b. GRANT NUMBER

5c. PROGRAM ELEMENT NUMBER
0602201

6. AUTHOR(S)

Steven E. Olson (University of Dayton Research Institute)
Martin P. DeSimio (ATK Space Systems and Sensors)
Mark M. Derriso (AFRL/VASA)

5d. PROJECT NUMBER
A01K

5e. TASK NUMBER

5f. WORK UNIT NUMBER
0E

7. PERFORMING ORGANIZATION NAME(S) AND ADDRESS(ES)

University of Dayton Research Institute
300 College Park
Dayton, OH 45469

ATK Space Systems and Sensors
3975 Research Blvd.
Dayton, OH 45430

Advanced Structural Concepts Branch (AFRL/VASA)
Structures Division
Air Vehicles Directorate
Air Force Materiel Command, Air Force Research Laboratory
Wright-Patterson Air Force Base, OH 45433-7542

8. PERFORMING ORGANIZATION REPORT NUMBER
AFRL-VA-WP-TP-2006-322

9. SPONSORING/MONITORING AGENCY NAME(S) AND ADDRESS(ES)

Air Vehicles Directorate
Air Force Research Laboratory
Air Force Materiel Command
Wright-Patterson Air Force Base, OH 45433-7542

10. SPONSORING/MONITORING AGENCY ACRONYM(S)
AFRL-VA-WP

11. SPONSORING/MONITORING AGENCY REPORT NUMBER(S)
AFRL-VA-WP-TP-2006-322

12. DISTRIBUTION/AVAILABILITY STATEMENT

Approved for public release; distribution is unlimited.

13. SUPPLEMENTARY NOTES

This work has been submitted to the Journal of Vibration and Acoustics, the American Society of Mechanical Engineers, publisher.

Report contains color. PAO Case Number: AFRL/WS 06-1131 (cleared May 01, 2006).

14. ABSTRACT

This paper explores how beamforming using Lamb waves can be used to benefit Structural Health Monitoring.

15. SUBJECT TERMS

Structural Health Monitoring, Piezoelectric Sensors, Beamforming

16. SECURITY CLASSIFICATION OF:			17. LIMITATION OF ABSTRACT:	18. NUMBER OF PAGES	19a. NAME OF RESPONSIBLE PERSON (Monitor)
a. REPORT	b. ABSTRACT	c. THIS PAGE			Lt. Emilio Talipan
Unclassified	Unclassified	Unclassified	SAR	16	19b. TELEPHONE NUMBER *(Include Area Code)* N/A

Standard Form 298 (Rev. 8-98)
Prescribed by ANSI Std. Z39-18

Submission to: Journal of Vibration and Acoustics

BEAMFORMING OF LAMB WAVES FOR STRUCTURAL HEALTH MONITORING

Steven E. Olson
Senior Research Engineer
University of Dayton Research Institute
Dayton, OH 45430

Martin P. DeSimio
Senior Research Engineer
ATK Space Systems and Sensors
Dayton, OH 45430

Mark M. Derriso
SHM Team Lead
Air Vehicles Directorate
Air Force Research Laboratory
WPAFB, OH 45433

ABSTRACT

Structural health monitoring techniques are being developed to reduce operations and support costs, increase availability, and maintain safety of current and future air vehicle systems. The use of Lamb waves, guided elastic waves in a plate, has shown promise in detecting localized damage, such as cracking or corrosion, due to the short wavelengths of the propagating waves. The use of such techniques for structural health monitoring of simple plate and shell structures has been demonstrated. However, most aerospace structures are significantly more complex and advanced techniques may be required. One advanced technique involves using an array of piezoelectric transducers to generate or sense elastic waves in the structure under inspection. By adjusting the spacing and/or phasing between the piezoelectric transducers, transmitted or received waves can be focused in a specific direction. This paper presents details on the analytical modeling and experimental testing of beamforming, using an array of piezoelectric transducers on an aluminum panel. Results are shown to compare well with theoretical predictions.

INTRODUCTION

Structural health monitoring (SHM) techniques are being developed to reduce operations and support costs, increase availability, and maintain safety of current and future air vehicle systems. SHM refers to automated methods for determining adverse changes in the integrity of mechanical systems [1]. In the literature, the capability of SHM systems is typically broken down into the following levels of increasing difficulty: (1) damage detection; (2) damage localization; (3) damage assessment; and, (4) life prediction. In general, SHM is accomplished as follows. The structure under investigation is excited using actuators (active SHM) or operational loading (passive SHM). The response to the excitation is sensed at various locations throughout the structure. The response signals (and possibly the excitation signal) are collected and processed. Based on the processed data, the state of the structure is diagnosed.

Various SHM techniques have been investigated depending on the scale of the damage to be detected. For example, damage such as fastener failure may have a more global effect on the structural dynamics and therefore modal-based damage detection techniques may be suitable. This paper focuses on detecting smaller scale damage, such as cracking or corrosion, which typically has a highly localized effect on the system dynamics. The use of Lamb waves, guided elastic waves in a plate, has shown promise in detecting such highly localized damage due to the relatively short wavelengths of the propagating waves. However, the Lamb wave behavior is fairly complex as the waves are dispersive and various modes may coexist [2].

Lamb waves are guided elastic waves that occur in a free plate. Because of their behavior, Lamb waves are particularly useful for investigating damage in plate and shell structures. Lamb waves can exhibit symmetric and antisymmetric waveforms, based on whether the out-of-plane displacements on either side of the plate are in or out of phase. As guided waves, Lamb waves are dispersive, meaning that the wave speed is a function of frequency. Due to dispersion, Lamb waves become distorted as they propagate. This results in

various waves with slightly different frequencies and wavelengths being excited in a structure. These waves interact and the resulting wave propagates at a group velocity which may differ from the individual phase velocities. For damage detection purposes, the group velocity can be thought of as the signal velocity, or the velocity at which energy is conveyed through a structure.

As frequency increases, the number of simultaneously existing waveforms also increases. To limit the number of coexisting waveforms, the excitation frequency is typically kept relatively low such that only the S_0 and A_0 waveforms will exist. These waveforms, S_0 and A_0, are referred to as the fundamental modes and are typically used for Lamb wave damage detection. For damage detection purposes, it is also useful to analyze only a single waveform. As a general rule, elastic waves can be used to detect damage on the order of the wavelength. The A_0 Lamb mode has a lower wave speed than the S_0 mode. The A_0 mode therefore has a smaller wavelength, and is more sensitive to smaller levels of damage. Conversely, the symmetric waveform has a substantially greater group velocity and would therefore arrive at a sensor well before the antisymmetric waveform. As a result, reflections of the S_0 wave may arrive at a sensor simultaneously with the initial A_0 wave, corrupting the measured signal. Giurgiutiu [3] has shown that, by adjusting the excitation frequency, it is possible to tune certain transducers to excite a single mode (either S_0 or A_0) dominantly.

The use of Lamb wave techniques to detect damage in simple plate and shell structures has been demonstrated [ref?]. However, most aerospace structures are significantly more complex and advanced techniques may be required. One advanced technique involves using an array of piezoelectric transducers to generate or sense elastic waves in the structure under inspection. By adjusting the spacing and/or phasing between the piezoelectric transducers, the transmitted or received waves can be focused in a specific direction. This focusing enhances signal quality (increases signal-to-noise ratio) and may improve the ability to locate damage by utilizing the focusing direction. This paper presents details relating to beamforming techniques using transmitting or receiving arrays. In the following sections, experimental testing and analytical modeling of Lamb wave propagation are discussed. Subsequent sections address the use of receiving and transmitting arrays, compare experimental measurements and analytical predictions with theoretical calculations, and introduce adaptive arrays. Finally, conclusions are made based on the results from these studies.

EXPERIMENTAL TESTING

To demonstrate the utility of Lamb waves for damage detection, experimental studies have been performed and measured results compared with theoretical values as well as simulated results from analytical modeling. Figure 1 shows a schematic of an aluminum plate specimen used for the experimental Lamb wave studies. The specimen consists of a sheet of 2024 aluminum with a thickness of 1.0 mm.

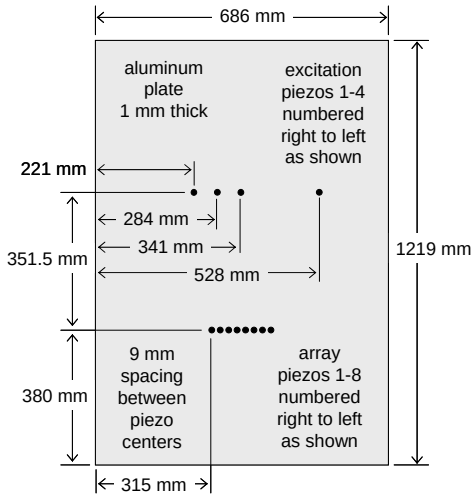

Fig. 1 Aluminum plate test article showing locations of piezoelectric transducers (drawing not to scale)

A collinear array of eight piezoelectric transducers is located at approximately one-third of the plate height. Four individual piezoelectric transducers are located at approximately two-thirds of the plate height. These four piezoelectric transducers are at angles of approximately 63°, 91°, 100°, and 110° relative to the center of the array. All of the individual piezoelectric transducers can be used to either excite the structure or sense the response. The piezoelectric transducers used for these studies are lead zirconate titanate (PZT) discs with a diameter of 6.35 mm and a thickness of 0.254 mm. The transducers have been bonded to the surface of the aluminum plate using M-Bond 200 adhesive. The piezoelectric discs are thickness poled and operate in a radial extension mode, such that an applied voltage across the thickness of the ceramic disc results in a radial expansion or contraction of the disc. Conversely, a radial expansion or contraction of the disc (i.e., a radial strain) creates a voltage potential across the thickness of the disc.

The excitation signals sent to the piezoelectric transducers to excite Lamb waves are typically Hanning-windowed sine bursts. Rather than continuous signals, pulses of three to seven waves are typically used to allow time of flight calculations and prevent unwanted interference between waves. A pulse with more cycles has higher energy than a pulse with fewer cycles. However, pulses with more cycles increase the likelihood that reflections may occur and interfere with the measured response. Often an additional ½ cycle is added to an integer number of cycles to provide a peak at the center of the signal. The Hanning window is used to reduce the amount of energy at frequencies other than the excitation frequency. Figure 2 shows an example of a five cycle Hanning-windowed sine

burst at 300 kHz, along with the frequency content of the signal.

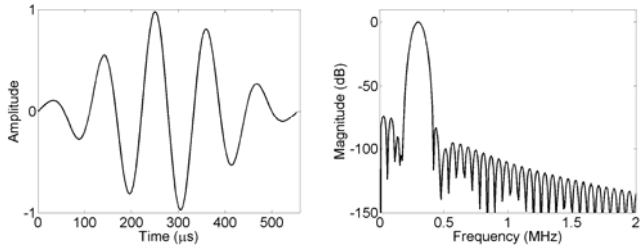

(a) (b)

Fig. 2 Five cycle Hanning-windowed sine burst time signal (a) and frequency content of the signal (b)

As discussed in following sections, the array of piezoelectric transducers can be used to receive or transmit Lamb waves. When a receiving array is utilized, a Hanning-windowed sine wave excitation signal is generated using an Agilent 33250A Function Generator. This signal is sent directly to one of the four upper piezoelectric transducers. Responses from the array of piezoelectric transducers are captured using a Windows-based PC with a data acquisition card. MATLAB routines are used to process the measured responses.

A similar setup is used for a transmitting array where eight separate signals of different phases must be generated. To reduce the cost of the equipment necessary to generate such signals, a digital waveform generating card has been utilized. However, the card is only capable of generating square wave signals, which results in greater spread of the frequency content in the excitation signal. Figure 3 shows a five cycle square wave burst at 300 kHz and the frequency content of the signal. Note that the square wave burst contains a much larger spread in frequencies than the Hanning-windowed sine wave burst shown in Figure 2b. In addition to the main peak centered at 300 kHz, the third and fifth harmonics are clearly visible in the spectrum shown in Figure 3b. However, the energy from these harmonics is more than 20 dB below the main peak energy. Therefore, reasonable Lamb wave signals can be generated from the square wave excitation. The Agilent 33250A Function Generator is used to provide clocking for the digital waveform generating card. Signals from the card are sent through an amplifier to increase the signal voltage and then to appropriate piezoelectric transducers in the array. The eight channel amplifier has been fabricated in-house to provide up to 75 volt peak-to-peak amplification of the excitation signals. Responses at each of the four individual piezoelectric transducers are captured using a Windows-based PC with a data acquisition card. MATLAB routines are used to process the measured responses.

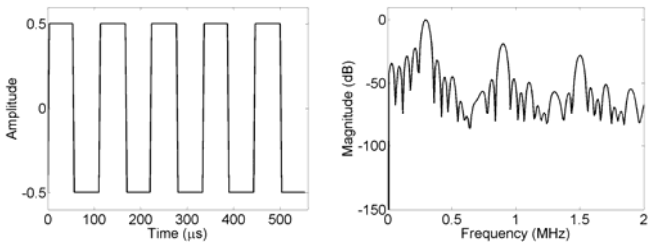

(a) (b)

Fig. 3 Five cycle square wave burst time signal (a) and frequency content of the signal (b)

For all of the studies discussed in this paper, excitation signals at 300 kHz have been utilized. Prior to performing beamforming, the group velocity of 300 kHz Lamb waves in the specimen must be determined. The velocity of the Lamb wave determines the time of arrival of signal energy at each element in the array. To calculate the velocity, Lamb waves are generated independently at each of the four upper piezoelectric transducers and the time of flight for the waves to arrive at each transducer in the eight element receiving array is measured. Dividing the distance traveled by the time of flight provides the group velocity. Since four transmitting and eight receiving piezoelectric transducers are used, 32 group velocity measurements are obtained. The average of the 32 measurements is used as the nominal group velocity in subsequent calculations.

Since experiments are conducted at a relatively low frequency-thickness product (0.3 MHz-mm) only the fundamental S_0 and A_0 waves are generated. Because the group velocity of the S_0 mode is approximately twice that of the A_0 mode, attention can be focused on solely the S_0 mode by time gating the response signals. The time gate is determined by examining the signal responses and selecting the interval corresponding to the S_0 pulse. Subsequent analysis is performed using the gated signals.

The time of flight is found as the time difference between the mid-energy points of the received and transmitted pulse bursts. The mid-energy point is the time at which 50% of the cumulative energy of a signal occurs. In practice, the cumulative distribution function (CDF) of the pulse energy is calculated and linear interpolation is used to find the time corresponding to 0.50 on the energy CDF. Since the excitation signal is identical for all of the group velocity experiments, a single excitation signal has been recorded and its mid-energy point used for all time of flight calculations. Table 1 lists the measured group velocities between all pairs of transmitting and receiving piezoelectric transducers. The average group velocity is 5.5 mm/μsec.

Table 1. Measured group velocities (mm/μsec)

	Rec 1	Rec 2	Rec 3	Rec 4	Rec 5	Rec 6	Rec 7	Rec 8
Exc 1	5.49	5.49	5.50	5.51	5.46	5.47	5.40	5.41
Exc 2	5.49	5.50	5.49	5.50	5.48	5.49	5.50	5.51
Exc 3	5.47	5.48	5.49	5.49	5.45	5.46	5.46	5.48
Exc 4	5.43	5.45	5.46	5.45	5.44	5.46	5.46	5.46

Beamforming can be accomplished by adjusting the spacing and/or phasing between the piezoelectric transducers in an array. For these experiments, the piezoelectric discs have been permanently adhered to the surface of the aluminum plate. As a result, the spacing is not easily changed so the phasing will be modified to focus the transmitted or received waves. However, it is still important to know the spacing between the various transducers with respect to the wavelength of the propagating waves. The wavelength, λ, can be found as:

$$\lambda = \frac{c}{f} \tag{1}$$

where c is the propagation speed of the waves and f is the frequency of the waves. Based on the measured propagation speed of 5.5 mm/μsec and the excitation frequency of 300 kHz, the wavelength can be calculated to be 18.3 mm. The piezoelectric transducers are spaced 9.0 mm, or approximately a half wavelength between adjacent elements in the array. For the theoretical calculations discussed in following sections, a half wavelength spacing has been assumed.

ANALYTICAL MODELING

In order to design accurate and efficient SHM systems, physics-based models are useful to provide a detailed understanding of the structural dynamics. Major advantages of analytical modeling over experimental testing include the ability to investigate different wave propagation cases relatively quickly, as well as the capability to examine the wave behavior through the entire thickness of the material (rather than solely based on surface measurements) or in locations not easily accessible for testing. One approach to model Lamb wave propagation is to numerically solve the governing wave equations with the appropriate boundary conditions. This approach can be taken for simple geometries, but becomes difficult for more complicated geometries or when damage is included. In such cases, different computational techniques can be used to analyze wave propagation. Explicit finite element methods, which step through the solution in time, are one of the more popular techniques, since numerous finite element codes exist and it is not necessary to develop specialized code.

For these studies, finite element simulations have been performed using ABAQUS/Explicit [4], an explicit time integration finite element code based on the central difference method. Analyses have been performed using models containing four-node, bilinear shell elements (S4R elements in ABAQUS). In the laboratory, Lamb waves are excited using surface-mounted piezoelectric transducers which are bonded to the plate at the locations shown in Figure 1. In the models, excitation is accomplished using point forces and moments at nodes which correspond to locations around the perimeter of the piezoelectric discs. Moments are required since the midplane of the aluminum plate is modeled, but the discs are attached to the outer surface of the structure. The piezoelectric discs are not explicitly modeled and any contribution to the mass or stiffness of the structure due to the discs is assumed to be negligible. In the laboratory, the piezoelectric discs also are used to sense the strains created due to the Lamb waves. In the models, the radial strain experienced by a disc is taken to be proportional to the measured output voltage of a piezoelectric transducer. Scaled voltage versus time data is extracted from the analytical results and can be processed using the same methods and routines used to process the experimental data. Earlier studies have demonstrated the utility of these modeling techniques [5].

RECEIVING ARRAY

As previously discussed, aerospace structures are typically more complex than simple plate and shell structures and advanced SHM techniques are required. One advanced techniques involves using an array of piezoelectric transducers to generate or sense elastic waves in the structure under inspection. An array is a collection of spatially distributed transmitting or receiving elements, used to concentrate energy in a specific angular region [6]. A brief description of array operation is given below.

Fundamental array operation is described based on receiving sinusoidal energy in the form of plane waves. For design purposes, arrays are typically assumed to consist of omnidirectional elements which, by definition, receive energy equally well from all directions. Figure 4 shows an array of two identical omnidirectional elements separated by a half wavelength. The output of the array, r(t), is obtained by adding the signals received at each element, $r_1(t)$ and $r_2(t)$. Waves arriving from 90° will reach both elements simultaneously, so the array output will be twice the signal received at either element. Since the elements are spaced a half wavelength apart, the responses, $r_1(t)$ and $r_2(t)$, to waves arriving from 0° will be 180° out of phase. Therefore, the array output signal will be zero. In general, for a wave arriving at an angle, θ, there will be a time delay between the signals at each element proportional to the additional propagation distance, l, where:

$$l = \left(\frac{\lambda}{2}\right)\cos(\theta) \tag{2}$$

The time delay, δ, can be found by dividing the propagation distance, l, by the wave speed, c.

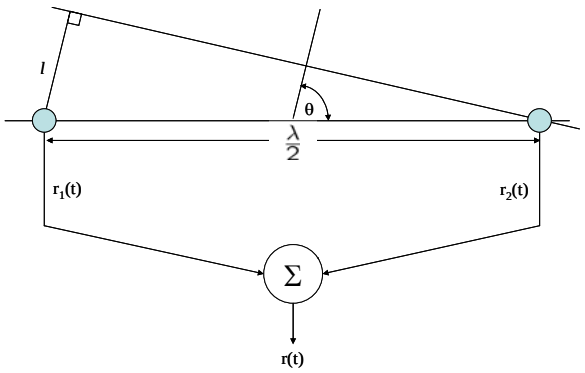

Fig. 4 Array of two identical omnidirectional elements

To illustrate the directional properties of arrays, polar plots of the received signal amplitude versus angle of arrival – called gain patterns – are created. The lobe of a gain pattern with the largest magnitude is referred to as the main lobe and the look angle refers to the angular orientation of the main lobe. Any lobes other than the main lobe are referred to as side lobes, and null angles occur in the directions where the array pattern equals zero.

It can be shown that the gain pattern for a linear array of N elements with half wavelength spacing is:

$$A(\theta) = \frac{\sin\left[\frac{N\pi}{2}\cos(\theta)\right]}{\sin\left[\frac{\pi}{2}\cos(\theta)\right]} \qquad (3)$$

where θ is the angle of arrival [6]. The gain patterns for linear arrays with two and eight element are shown in Figure 5. To facilitate comparisons in this paper, the maximum value in each gain pattern has been normalized to unity.

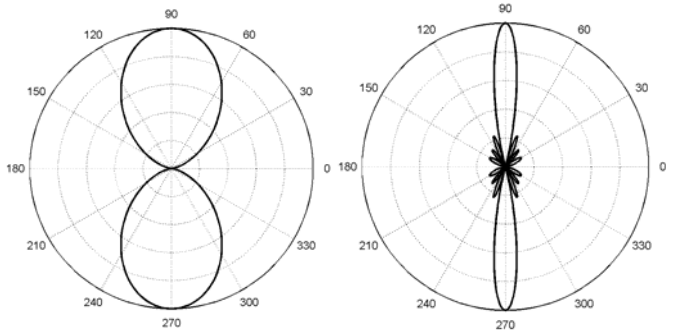

Fig. 5 Theoretical gain patterns for two and eight element arrays

The mainlobe of the linear arrays described above will always be perpendicular to the axis of the elements. However, by adding phase shifts to the signals from each element, the mainlobe can be pointed in any direction. This process is known as beamsteering. A diagram of an eight element linear array with a half wavelength spacing between elements and with delays to enable beamsteering is shown in Figure 6. The fundamental delay time is shown as δ. Arbitrarily assigning the rightmost element in the array to receive zero delay, each successive element to the left receives an additional delay of δ.

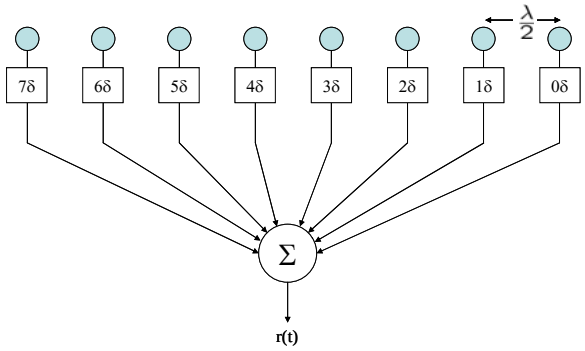

Fig. 6 Functional diagram of a receiving array

The mainlobe orientation or look angle, θ, as a function of the delay, δ, is [6]:

$$\theta = \cos^{-1}\left(\frac{c\delta}{d}\right) \qquad (4)$$

where c is the wavespeed and d is the spacing between array elements. By definition, $c = \lambda \cdot f$ and $f = 1 / T_0$, where T_0 is the period of the wave energy. For a half wavelength spacing (i.e., $d = \lambda / 2$) the look angle becomes:

$$\theta = \cos^{-1}\left(\frac{2\delta}{T_0}\right) \qquad (5)$$

As shown in Equation 5, the look angle is controlled by the ratio of the time delay to the period of the signal. The mainlobe can be electronically steered by computing the array output for delay values ranging from 0 to $T_0 / 2$. Figure 7 shows a plot of the look angle versus the normalized delay ratio (δ / T_0). In practice, beamforming with a receiving array is done with digital signal processing of sampled signals. A MATLAB function has been developed to provide arbitrary, non-integer sample period delays according to the digital filter method of Oppenheim and Schafer [7].

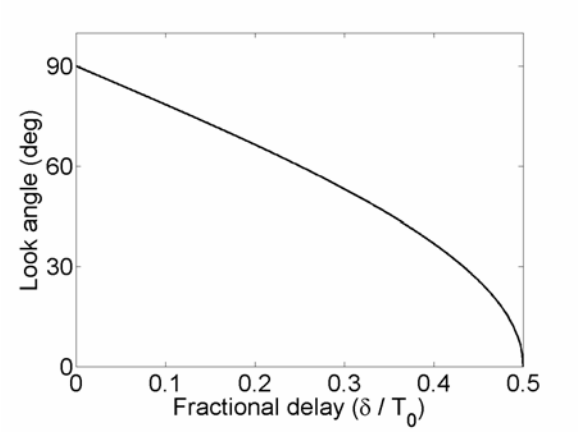

Fig. 7 Look angle versus normalized delay.

The experimental test article uses an eight element collinear array with half wavelength spaced elements. Theoretical gain patterns for an eight element array with δ set to obtain look angles matching the angles to the four individual piezoelectric transducers are shown in Figure 8.

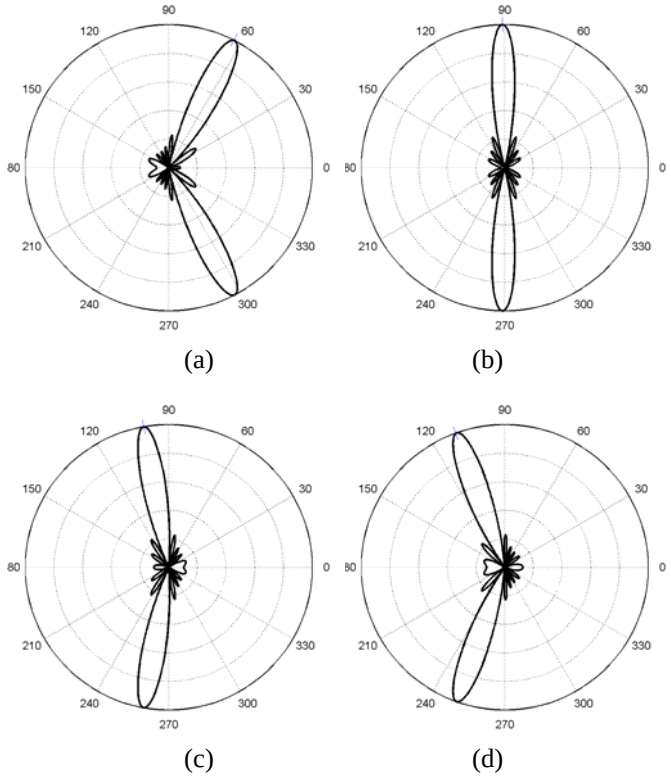

Fig. 8 Theoretical gain patterns using eight element receiving array for look angles of (a) 63°, (b) 91°, (c) 100°, and (d) 110°

Gain patterns of the array used in the experiment have been measured as follows. One of the four upper piezoelectric transducers transmits a pulse. The receiving array is operated with the appropriate delays to provide look angles from 0° to 359° in 1° increments. The energy of the array output signal is computed over the time interval corresponding to the arrival of the S_0 wave. An experimental gain plot is obtained by plotting the square root of the received pulse energy as a function of look angle. Plots of received signal level versus look angle are shown in Figure 9. Gain patterns are shown corresponding to transmission from individual piezoelectric discs at 63°, 91°, 100°, and 110°.

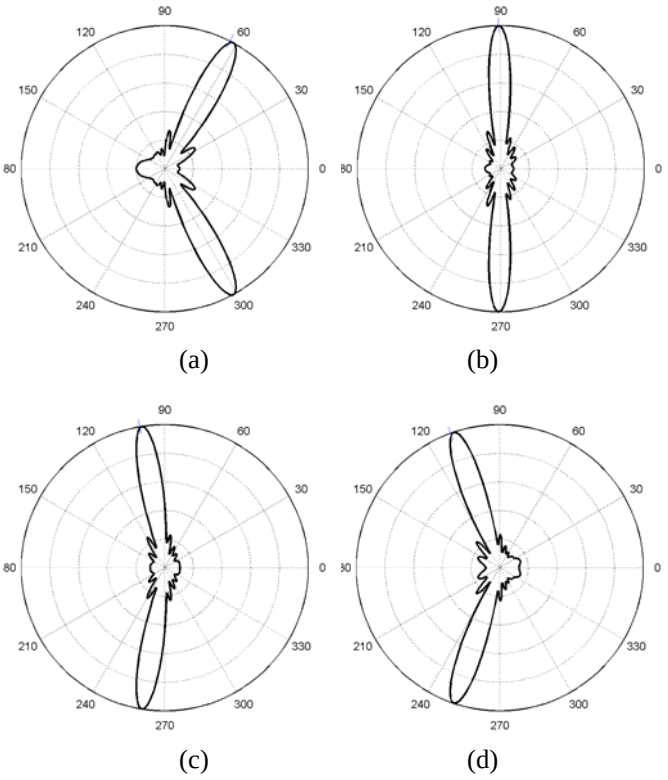

Fig. 9 Measured gain patterns using eight element receiving array for transmitting piezoelectrics at angles of (a) 63°, (b) 91°, (c) 100°, and (d) 110°

Similar to the experimental testing, finite element simulations have been performed where each of the four upper piezoelectric transducers transmits a pulse. The response of each element in the array, due to excitation from an individual piezoelectric disc, has been calculated. Appropriate delays have been added to each channel of simulated data to provide beamsteering. Plots of simulation results for received signal level versus look angle are shown in Figure 10. Gain patterns are shown corresponding to transmission from individual piezoelectric discs at 63°, 91°, 100°, and 110°.

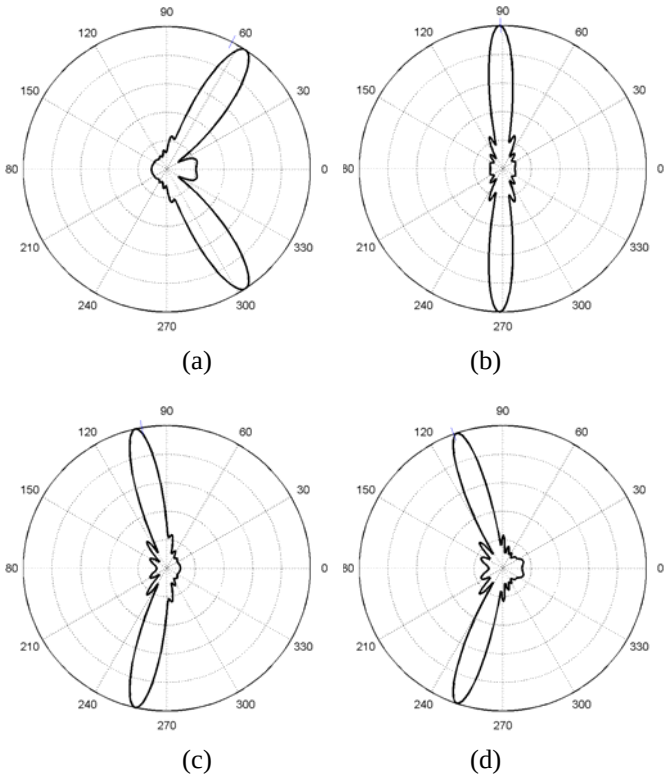

Fig. 10 Simulated gain patterns using eight element receiving array for transmitting piezoelectrics at angles of (a) 63°, (b) 91°, (c) 100°, and (d) 110°

TRANSMITTING ARRAY

Beamforming can also be utilized for transmitting arrays. Time delays are applied to the excitation signal sent to each element in the array to focus the transmitted energy in a specific direction. Figure 11 shows an example of a transmitting array. As shown in the figure, delayed versions of the excitation signal are applied to adjacent elements in the array. The look angle of the transmitted energy is determined by the same relationship used to calculate the look angle of the receiving arrays discussed above. Therefore, the theoretical gain patterns for the transmitting arrays will be identical to those shown previously in Figure 8 for the receiving arrays.

For experimental studies using transmitting arrays, a digital waveform generating card has been utilized to reduce the cost of the equipment necessary to generate multiple channel sinusoids with precise phase control. A National Instruments NI PXI-6542 digital waveform generator card provides eight replicas of a five cycle square wave. The digital waveforms are created with 60 samples per cycle. Delays of +30 to -30 samples steer the mainlobe from 0° to 180°.

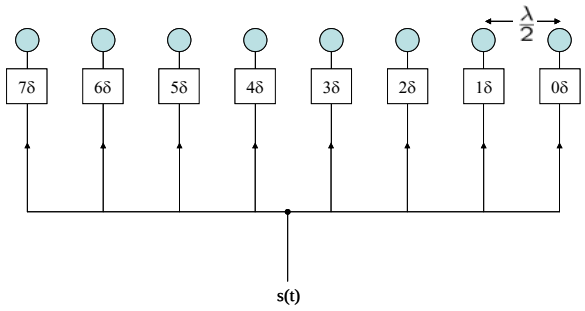

Fig. 11 Functional diagram of a transmitting array

To assess the effectiveness of experimental beamforming, gain patterns of the transmitted signals have been computed. Five cycle square wave pulses at the 300 kHz fundamental frequency are used to excite each element in the array. Experiments have been performed using arrays with each of the possible 60 delay values to provide results with the mainlobe steered from 0° to 180°. For each delay value, responses at each of the four upper piezoelectric transducers are recorded. As with the receiving arrays, the time interval corresponding to the arrival of the S_0 mode has been identified, and the energy of each recorded signal is computed over this interval. Gain patterns at each individual transducer are obtained by plotting the square root of the computed energy versus the look angle determined by the given delay value. Figure 12 shows the measured gain patterns found by this method.

Analytical gain pattern plots could be created using the same process utilized for the experimental studies. However, such plots have not been created due, in part, to the large number of analyses which would be required to create detailed plots. In addition, preliminary analytical simulations using square wave excitation have produced poor results, likely due to the stepped forces and moments applied in the model. Analytical studies of transmitting arrays are continuing.

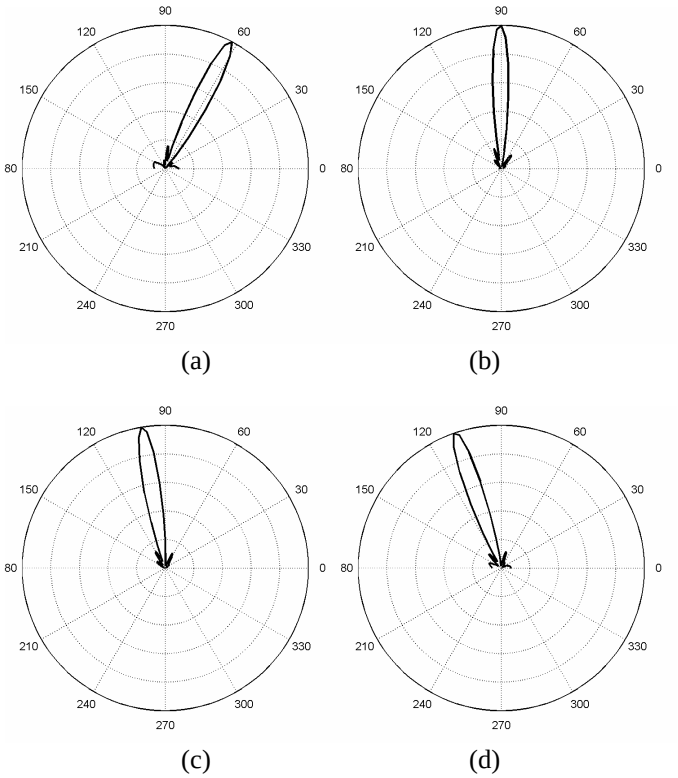

Fig. 12 Measured gain patterns using eight-element transmitting array for look angles of (a) 63°, (b) 91°, (c) 100°, and (d) 110°

ADAPTIVE ARRAYS

Adaptive beamforming uses adjustable weights to modify the gain pattern for narrowband signals. SHM systems may benefit from the capability of adaptive arrays to perform automatic, online adaptation to changing environmental conditions (e.g. the capability to reduce the effects of noise from time-varying locations). A functional block diagram of an adaptive receiving array is shown in Figure 13. Signals are received at each sensor and then split into in-phase and quadrature paths. The in-phase path is the signal from the sensor, and the quadrature path adds a 90° phase shift (based on an assumed center frequency of the received narrowband signal) to the received signal. The in-phase and quadrature signals are multiplied by adjustable weight values and then added to obtain the output of the array. The weights can be computed using the least mean squares (LMS) or other algorithms. A complete discussion of the LMS algorithm and its application to adaptive beamforming can be found in [8].

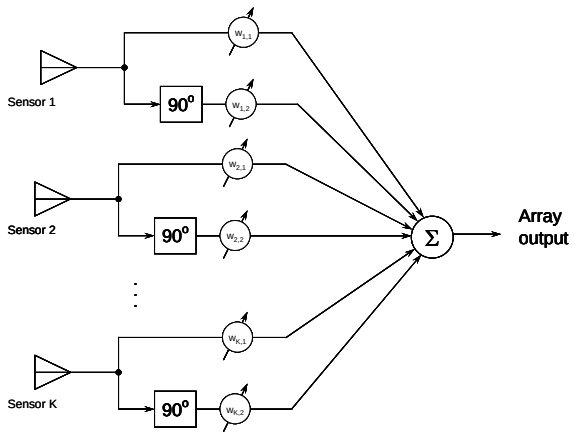

Fig. 13 Functional diagram of an adaptive array

Adaptive arrays are useful for generating customized array patterns. For example, an array with seven uniformly spaced elements will have a main lobe at 90° and significant side lobes at 45° and 135°. Assuming a noise source appears at 45°, using an adaptive array it is possible to compute weight values such that a desired signal at 90° is received at full strength while simultaneously reducing gain of the noise by more than 20 dB. Array patterns for a uniform array with and without the noise canceling notch are shown in Figure 14 (shown on a Cartesian plot to better illustrate the noise canceling notch at 45°).

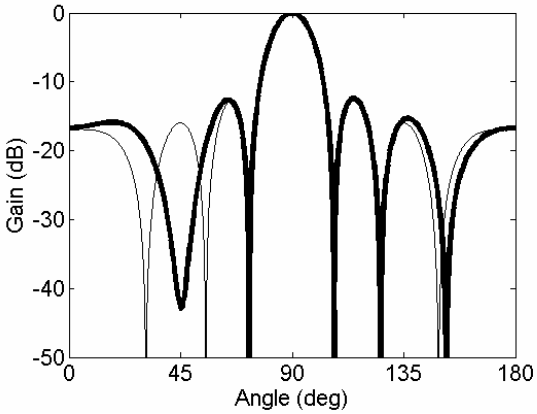

Fig. 14 Gain patterns for seven element, uniformly-spaced collinear arrays, with (heavy line) and without (thin line) weights corresponding to a noise canceling notch at 45°

DISCUSSION

For receiving arrays, good agreement is generally seen between the theoretical, experimental, and simulated gain patterns shown in Figures 8, 9, and 10, respectively. The overall structures of the gain patterns compare well across the three methods; however, the experimental and simulated look angles differ slightly from the theoretical look angle. A slight difference is seen between the experimental and theoretical results, as the root mean square (RMS) error in the look angle

is only 1.2°. Considerably more variation is seen in the analytical results, although the RMS error in the look angle is still only 4.1°. These differences are due, in part, to inaccuracy in the piezoelectric transducer spacing. Recall that the theoretical calculations assume a half wavelength spacing while the actual experimental spacing is slightly greater. In addition, the group velocity in the analytical simulations may differ somewhat from the theoretical or experimental group velocities depending on the material properties utilized for the simulations. Regardless, the theoretical and analytical results generally provide a good first approximation of the actual beamforming behavior and illustrate the potential benefits of receiving arrays.

Good agreement is also seen between the theoretical and experimental gain patterns for transmitting arrays. As with the receiving arrays, the overall structures of the experimental gain patterns shown in Figure 12 compare well with the theoretical gain patterns from Figure 8. However, the experimental look angles again differ slightly from the theoretical look angles. These differences result due, at least in part, to the inaccuracy of the piezoelectric transducer spacing assumed for the theoretical calculations. Preliminary analytical simulations using square wave excitation have produced poor results, likely due to the stepped forces and moments applied in the model. Analytical studies of transmitting arrays are continuing.

Lastly, a brief introduction has been given to adaptive arrays where adjustable weights are used to modify the gain for narrowband signals. Adaptive arrays are useful for generating customized array patterns and may prove extremely beneficial for SHM applications to cancel out noise from known sources or unwanted wave reflections (e.g. off the free edges of a plate rather than from damage). It is anticipated that adaptive arrays will enhance standard beamforming arrays by allowing additional tuning for improved performance.

CONCLUSIONS

SHM techniques are being developed to reduce operations and support costs, increase availability, and maintain safety of current and future air vehicle systems. The use of Lamb waves has shown promise in detecting localized damage, such as cracking or corrosion. For improved damage detection, advanced techniques, such as using arrays of piezoelectric transducers to receive or transmit signals, are being investigated. By adjusting the spacing and/or phasing between the piezoelectric transducers, transmitted or received waves can be focused in a specific direction. This focusing enhances signal quality (increases signal-to-noise ratio) and may improve the ability to locate damage by utilizing the focusing direction. Experiments demonstrate successful beamforming with Lamb wave signals in an aluminum plate for both receiving and transmitting arrays. Finite element analysis has been shown to provide a good first approximation of the beamforming behavior. Results from the experiments and analytical simulations compare well with theoretical calculations. Adaptive arrays, using adjustable weights, may further improve SHM system performance by providing a degree of robustness to operational noise sources.

ACKNOWLEDGMENTS

These investigations have been performed at the Air Vehicles Directorate of the Air Force Research Laboratory. The efforts of S. Olson and M. DeSimio have been performed under Air Force Contract Number FA8650-04-D-3446. The authors wish to acknowledge the support of Mr. Todd Bussey, for setting up the instrumentation and collecting experimental measurements, and Lt. Dustin Thomas, for designing the hardware layout to perform transmitter beamsteering. Their assistance with the experiments discussed in this paper is greatly appreciated.

REFERENCES

[1] Sohn, H. and Farrar, C., 2001, “Damage Diagnosis Using Time Series Analysis of Vibration Signals,” Smart Mater Struct, 10(3): pp. 446-451.

[2] Rose, J.L., 1999, Ultrasonic Waves in Solid Media, Cambridge University Press, Cambridge, MA.

[3] Giurtiugiu, V., 2005, “Tuned Lamb Wave Excitation and Detection with Piezoelectric Wafer Active Sensors for Structural Health Monitoring,” J Intel Mat Syst Str, 16(4), pp. 291-305.

[4] ABAQUS Analysis User’s Manual, 2005, Version 6.5, ABAQUS, Inc., Providence, RI.

[5] Derriso, M.M, Olson, S.E., DeSimio, M.P., and Sanders, B., 2005, “Development of Automated Damage Detection Techniques,” Materials Damage Prognosis, J.M. Larsen, et al., ed., TMS, Warrendale, PA.

[6] Orfanidi, S.J., 2006, Electromagnetic Waves and Antennas, draft book available online at http://www.ece.rutgers.edu/~orfanidi/ewa/.

[7] Oppenheim, A. and Schafer, R., 1989, Discrete-Time Signal Processing, Prentice-Hall, Englewood Cliffs, NJ.

[8] Widrow, B. and Stearns, S.D., 1985, Adaptive Signal Processing, Prentice-Hall, Englewood Cliffs, NJ.